ARTICLE

Reactive Adsorption of NO_2 on Copper-Based Metal−Organic Framework and Graphite Oxide/Metal−Organic Framework Composites

Benoit Levasseur, Camille Petit, and Teresa J. Bandosz*

Department of Chemistry, The City College of New York and The Graduate School of CUNY, 160 Convent Avenue, New York, New York 10031, United States

ABSTRACT Composites of a copper-based metal−organic framework (MOF) and graphite oxide (GO) were tested for NO_2 adsorption and retention of NO in dry and moist conditions. The samples were analyzed before and after exposure to NO_2 by thermal analysis, Fourier transform infrared spectroscopy (FTIR), X-ray diffraction, and adsorption of nitrogen at −196 °C. In dry conditions, the composites exhibit an enhanced NO_2 breakthrough capacity compared to MOF and GO separately. This improvement is linked to the increased porosity and the reactive adsorption of NO_2 on copper, which leads to the formation of bidentate and monodentate nitrate. Even though less NO_2 is adsorbed in moist conditions than in dry ones, the materials are more stable than in dry conditions and the NO retention is enhanced. Water in the challenge gas competes with NO_2 to bind to copper, and thus, the number of reactive adsorption sites on which NO_2 can be adsorbed/reacted decreases.

KEYWORDS: metal−organic framework • graphite oxide • composite • nitrogen dioxide • reactive adsorption • porosity • nitrate

1. INTRODUCTION

Energy consumption constantly increases following the increasing trend in human population and activity. Even though renewable sources of energy are explored and they become more and more important, the combustion of fossil fuels still fulfills the majority of energy requirements. Among the pollutants released during fossil fuel combustion are nitrogen oxides (NO_x) (1). This category of gas comprises NO and also NO_2 (more toxic than NO) which are involved in the formation of photochemical smog and acid rain (2). Because of its toxicity, efficient technologies to remove NO_x from air are needed.

The technology currently employed to "trap" NO_x is called selective catalytic reduction (SCR) and enables the conversion of NO_x into nitrogen and water (3). Nevertheless, this method suffers from some limitations as, for instance, the release of unreacted ammonia (used as a reductant in this process) and the requirement of high temperatures (4). Considering these issues, several research groups have focused their work on finding alternative methods to SCR. The most common one is the adsorption of NO_2 on a fixed bed adsorbent. Materials tested so far include activated carbons, activated carbon fibers (ACFs), sludge derived adsorbents or zeolites (both virgin and modified) (5−17). This approach almost inevitably leads to the reduction of NO_2 to NO along with the oxidation of the carbon surface (17, 18). Consequently, one can see that if the problems caused by NO_2 release can be solved via adsorption, the retention of NO remains an issue that needs to be addressed. To confront this complex problem, ways to reduce NO into nitrogen and oxygen have been studied. For instance, the impregnation of a carbon-based support with transition metals has been reported by several research groups (19−25). Among the inorganic species tested, copper appears as a promising one.

Metal−organic frameworks (MOFs) have emerged as a new class of materials which currently draw the attention of many scientists due to their high porosity and diversity of metallic component (26). MOFs are formed by the coordination of a metallic center and an organic ligand (mainly carboxylate and sulfonate) resulting in the creation of a well-defined 3D network (26). As in the case of activated carbons, the high porosity of MOFs has naturally directed their potential applications toward gas purification (27, 28). Various types of MOF have been tested for the removal of gases and vapors (27−31). Diverse performances were observed depending on the material selected which must be related to both chemistry (type of metal and organic ligand) and the structure (pore size) of the MOFs. The catalytic activity of these materials has been also widely investigated (26, 32). Studies reported the redox potential of MOFs and their interesting performances for the catalysis of various reactions (mainly hydrogenation and oxidation reactions) (32). Interestingly, to the best of our knowledge, the retention of NO_x on such materials has not been studied. Recently, the preparation of MOF/graphite oxide (GO) composites (33, 34) has been reported along with their application in the removal of a gas of basic nature (NH_3) (35, 36). A significant enhancement of the adsorption capacity of the composites compared

* To whom correspondence should be addressed. Tel: (212)650-6017. Fax: (212) 650-6107. E-mail: tbandosz@ ccny.cuny.edu.
Received for review August 26, 2010 and accepted October 26, 2010

DOI: 10.1021/am100790v

Published on Web 11/10/2010

to the parent materials was observed and linked to the increased dispersive forces in the pores of the composites compared to MOF and GO alone (35, 36). The importance of adsorbent porosity for NO_2 adsorption at ambient conditions has been recently pointed out (37).

Considering the above, the objective of this study is to test copper-based MOF/GO composites (34) for the adsorption of NO_2 and the retention of NO in dry and moist conditions. The performances of these samples are compared to the ones of the parent materials and discussed in order to elaborate NO_2 adsorption mechanisms.

2. EXPERIMENTAL SECTION

2.1. Materials. The synthesis of the parent materials, referred to as HKUST-1 and GO, is described in detail in refs 34 and 38, respectively. The syntheses were done following Millward and co-workers (39) for HKSUT-1 and Hummers (40) for GO. HKUST-1 was prepared by mixing copper nitrate hemipentahydrate (10 g) and 1,3,5 benzenetricarboxylic acid (BTC) (5 g) in *N*,*N*-dimethylformamide (DMF, 85 mL) in ethanol (85 mL) and deionized water (85 mL). The mixture was then heated at 85 °C for 21 h under shaking. After cooling, the crystals were filtered, washed, and immersed in dichloromethane. Dichloromethane was changed twice during 3 days. The crystals were collected after filtration and washed with dichloromethane. Then, drying was performed by heating the crystals at 170 °C for 28 h under a vacuum. The resulting product was kept in a desiccator and is referred to as HKUST-1.

The preparation of the composites was done by adding varying amounts of GO powder to well-dissolved MOF precursors and solvent solution (the same procedure as in the preparation of HKUST-1). The resulting mixture was sonicated for 5 min and stirred for another 30 min, and then, the same synthesis procedure as that for HKUST-1 was carried out. The preparation of the composites whose GO content ranges from 5 to 18 wt % of the final material weight is addressed in ref 40. The composites are referred to as MG-*n* with $n = 1, 2$, and 3 for the different GO contents (5, 9, and 18 wt %, respectively).

2.2. Methods. 2.2.1. ***NO_2 Breakthrough Capacity.*** Evaluation of NO_2 sorption capacity was conducted in a laboratory-scale, fixed-bed reactor system, at room temperature and in dynamic conditions. In a typical test, a flow of NO_2 diluted with dry or moist (70% humidity) air went through a fixed bed of adsorbent with a total inlet flow rate of 225 mL/min and a NO_2 concentration of 1000 ppm. The adsorbent's bed was packed into a glass column (length 370 mm, internal diameter 9 mm) and consisted of about 2 cm^3 of glass beads well mixed with the amount of adsorbent required to obtain a homogeneous bed (between 50 and 120 mg). The beads were used to avoid the pressure drop and, thus, to favor the kinetics of the breakthrough tests. The concentrations of NO_2 and NO in the outlet gas were measured using an electrochemical sensor (RAE Systems, MultiRAE Plus PGM-50/5P). The adsorption capacity of each adsorbent was calculated in milligram per gram of adsorbent by integration of the area above the breakthrough curve. The tests were conducted until the concentrations of NO_2 and NO reached the electrochemical sensors' upper limit values of 20 and 200 ppm, respectively. Tests were implemented by diluting the NO_2 stream with either dry or moist air stream, respectively. After the breakthrough tests, all samples were exposed to a flow of carrier air only (180 mL/min) to evaluate the strength of NO_2 retention. The suffixes -ED and -EM are added to the name of the samples after exposure to NO_2 in dry and moist conditions, respectively.

2.2.2. ***Thermal Analysis.*** Thermogravimetric (TG) curves and their derivatives (DTG) were obtained using a TA Instrument

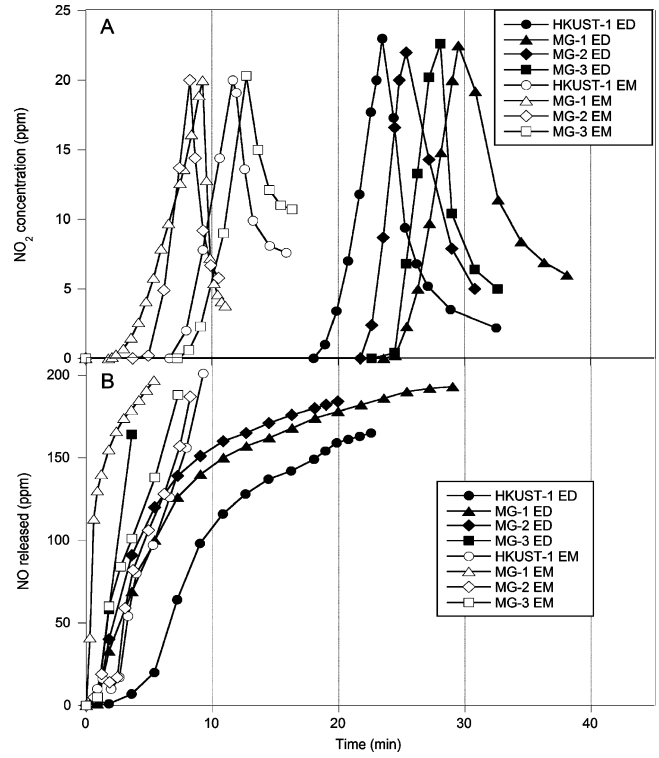

FIGURE 1. NO_2 breakthrough curves (A) and NO released during NO_2 adsorption process (B) on HKUST-1, MG-1, MG-2, and MG-3 materials in dry and moist conditions.

thermal analyzer. The samples (initial and exhausted) were previously dried in oven at 100 °C to remove moisture, and then, they were submitted to a regular increase of temperature, from 30 to 1000 °C, with a heating rate of 10 °C/min under a nitrogen flow held at 100 mL/min.

2.2.3. ***Fourier Transform Infrared Spectroscopy.*** Fourier transform infrared (FTIR) spectroscopy was carried out using a Nicolet Magna-IR 830 spectrometer using the smart diffuse reflectance method. The experiments were done on the powdered samples 2 to 3 wt % (initial and exhausted), with 97−98 wt % KBr addition. The spectrum was generated, collected 16 times, and corrected for the background noise with pure KBr spectra.

2.2.4. ***X-ray Diffraction.*** X-ray diffraction (XRD) measurements were conducted using standard powder diffraction procedures. Adsorbents (initial and exhausted) were ground with DMF (methanol for GO) in a small agate mortar. The mixture was smear-mounted onto a glass slide and then analyzed by Cu Kα radiation generated in a Philips X'Pert X-ray diffractometer. A diffraction experiment was run on a standard glass slide for the background correction.

2.2.5. ***Adsorption of Nitrogen.*** Nitrogen isotherms were measured at −196 °C using an ASAP 2010 (Micromeritics). Prior to each measurement, initial and exhausted samples were outgassed at 120 °C. The surface area, S_{BET}, the total pore volume, V_t, the micropore volume, V_{mic} (Dubinin−Radushkevich method (41)), and the mesopore volume, V_{mes}, were obtained from the isotherms.

3. RESULTS AND DISCUSSION

The NO_2 breakthrough curves of the materials studied are presented in Figure 1. The calculated capacities (*Q*) in dry and moist conditions are summarized in Table 1. It is important to notice that the *Q* values are not determined at an equilibrium; therefore, they can be considered as underestimated. As mentioned in the experimental part, NO_2

Table 1. NO_2 Adsorption Capacities (Q) and the Percentage of NO Released (R) for the HKUST-1, MG-1, MG-2, MG-3, and GO Materials in Dry and Moist Conditions

		dry conditions		moist conditions	
samples	GO content (%)	Q NO_2 (mg/g_{mat})	R (NO)[a] (%)	Q NO_2 (mg/g_{mat})	R (NO) (%)
HKUST-1	0	106 ± 1	9	54 ± 1	7
MG-1	5	134 ± 1	14	43 ± 2	9
MG-2	9	112 ± 1	13	38 ± 1	8
MG-3	18	124 ± 2	>18[b]	59 ± 3	5
GO	100	1.2		0.8	

[a] Amount of NO released during the adsorption process. [b] Estimation based on a prospective of polynomial fitting from the MG-3 NO curve (Figure 1).

adsorption was measured in dynamic conditions and we were not able to measure the whole breakthrough curves due to 20 ppm, detection limit of our sensor. In dry conditions, the measured NO_2 adsorption capacities are more than two times higher than those in moist conditions. The amounts adsorbed range between 106 mg/g on HKUST-1 and 134 mg/g on MG-1 in dry conditions. In moist conditions, values between 38 mg/g on MG-2 and 59 mg/g on MG-3 (Table 1) are reported. Generally speaking, there are not significant differences in the shapes of the NO_2 breakthrough curves. The fact that they are not very steep indicates the kinetic limitations, which might be related to chemical reactions. Nevertheless, similar slopes suggest similar mechanisms of reactive adsorption. Moreover, the slopes of the desorption curves indicate the similar strength of the NO_2 retentions. The addition of graphite oxide leads to an enhancement in the NO_2 capacity in dry conditions, since all the composite materials display a better performance than that of HKUST-1 (the following order is observed: MG-1 > MG-3 > MG-2 > HKUST-1). In contrast, in moist conditions, the addition of GO does not necessarily lead to an increase in the capacity. In this case, the amounts adsorbed follow the trend: MG-3 > HKUST-1 > MG-1 > MG-2. On the basis of the measured NO_2 adsorption capacities of the parent materials (HKUST-1 and GO) and the composition of adsorbents, the capacities for hypothetical physical mixtures for each composite sample were calculated. A comparison between the measured and hypothetical capacities (in mg/g) is shown in Figure 2. A very good performance of the composites in dry conditions indicates a beneficial synergy between the composite components. Such effect was found for NH_3 adsorption, and it was attributed to the increased volume of small pores as a result of the interaction between GO and HKUST-1, which led to increased dispersive forces (36). Briefly, it was found that the composites are formed by reactions between the functional groups of GO and the copper sites of HKUST-1. As a result of these interactions, a new porosity is created at the interface between the graphene layers and the MOF "blocks". This additional porosity was evidenced by hydrogen and nitrogen sorption (34). In these "new" pores, the dispersive forces are expected to be the strongest, owing to the dense arrays of atoms of GO, and consequently, the adsorption is favored/enhanced. On the other hand, in moist conditions, the experimentally measured amounts of NO_2 adsorbed are smaller than the hypothetical ones for all composites but MG-3. This suggests that water strongly modifies the adsorption mechanism of NO_2 on HKUST-1 and on the composite materials in comparison with the mechanism taking place in dry conditions. Taking into account the polar character of these two compounds, the competitive adsorption between water and NO_2 seems to be a plausible explanation. Such a view is in accordance with several studies, which indicate that both water (42, 43) and NO_2 (21, 44) can bind to copper, which results in the decrease in the number of adsorption centers. In dry conditions, where all these metallic sites are available for binding to NO_2, the optimum capacity can be reached.

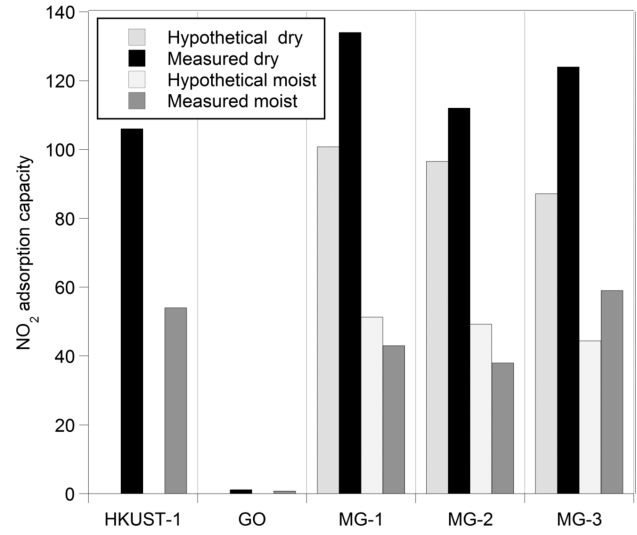

FIGURE 2. Measured and hypothetical NO_2 adsorption capacity for the HKUST-1, GO, MG-1, MG-2, and MG-3 materials.

Since a release of NO during NO_2 reactive adsorption can create an application problem, its concentration in the effluent was also monitored (Figure 1). The fraction of NO released (R) during NO_2 adsorption with respect to the amount of NO_2 adsorbed was calculated from the breakthrough curves, and it is reported in Table 1. Since this fraction in dry conditions increases with an increase in the content of GO component (from 9% for HKUST-1 to around 18% for MG-3), this activity is linked to the capability of the carbonaceous component to reduce NO_2 (45). In moist conditions, for all materials, less NO is released than in dry conditions. It is interesting that the amount of NO released decreases with an increase in the content of GO. This indicates that in moist conditions the reduction of NO_2 to NO is inhibited by the presence of graphene layers. Moisture

also slightly improves the performance toward NO on HKUST-1 compared to the dry environment.

Considering the results discussed above, the presence of water in the challenge gas decreases the NO_2 adsorption capacity due to the competition between water and NO_2 to bind to copper. At the same time, it prevents NO formation/release from the surface. Since the reduction of NO_2 to NO by the carbonaceous component should not be visibly affected by the presence of water, owing to the hydrophobicity of carbon materials, the formation of NO is likely caused by a mechanism/reaction other than the reduction of NO_2 by the carbon matrix. This is supported by the fact that, even in the absence of GO (see HKUST-1), NO is formed. A plausible explanation would be the adsorption of two NO_2 followed by a disproportionation reaction with formation of NO and nitrate. In the presence of water, the binding of NO_2 to the copper centers is limited, so less NO is formed. Thus, besides the GO component, MOF also contributes to the release of NO as a NO_2 reactive adsorption byproduct.

Since the surface features of the initial samples have been already described elsewhere (34), only the changes in the porosity which we refer to as a texture, as well as the chemical character of the surface observed after NO_2 exposure in dry and moist conditions, are discussed here, in order to understand the NO_2 reactive adsorption mechanism. To do it, the results obtained on the unexposed samples have to be compared to those obtained on the exhausted ones.

X-ray diffractograms of the fresh and exhausted samples are shown in Figure 3. It is interesting that, for all samples at all conditions, the structure of a parent material or composite can be considered as not significantly altered after the exposure to NO_2. Nevertheless, a general trend of a slight decrease in the intensity of the signals on the exhausted samples is observed, which indicates a partial destruction of the main framework. Among the materials studied, the MG-2 composite exhibits the most visible changes in structure after the NO_2 exposure in dry or moist conditions. This composite is also the least effective as a NO_2 adsorbent in both conditions. Surprisingly, the analysis of the NO_2 adsorption capacity in dry conditions and the analysis of the X-ray diffraction patterns after the exposure indicate that the structure is more preserved on the materials that display high NO_2 adsorption capacities. This is in a contradiction with the previous study, where the NH_3 adsorption on the same materials was analyzed (36). In moist conditions, the observed behavior is more complex. As in dry conditions, MG-2, which is the least effective material for NO_2 adsorption, seems to be the most damaged after the breakthrough test. For the other materials, no clear indication of the changes in the structure after the exposure to NO_2 can be found. This relationship between the activity and stability of the structure clearly shows that the adsorption is accompanied by chemical reactions, which lead to a partial destruction of the composite framework. This destruction

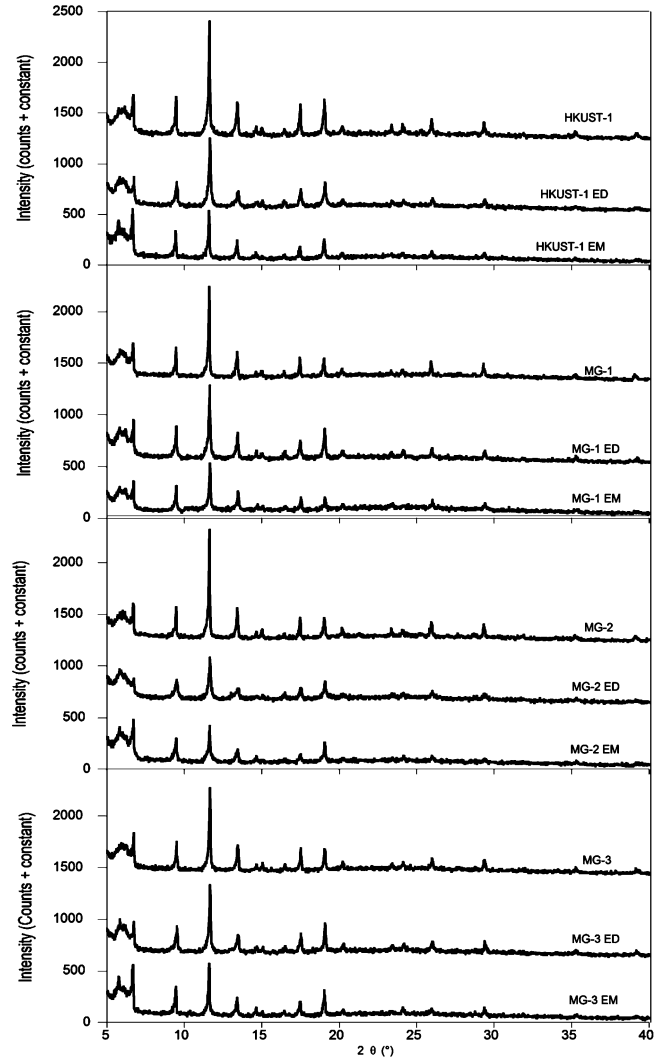

FIGURE 3. X-ray diffraction patterns of HKUST-1, MG-1, MG-2, and MG-3 before and after exposure to NO_2.

process results in a fast loss of NO_2 adsorption capacity, which is especially visible for MG-2 and HKUST-1 run in dry conditions.

The parameters of the porous structure calculated from the nitrogen adsorption isotherms are summarized in Table 2. As seen, a significant decrease in the surface area is found for the samples exposed to NO_2 in dry conditions. On HKUST-1, S_{BET} decreases from 909 to 63 m^2/g (about 90% decrease) in dry conditions. It is important to mention that this sample is the least effective adsorbent for NO_2. Concerning the composite materials, their specific surface area decreased by 80% after the exposure to NO_2 in dry conditions. In moist conditions, only 20% of the specific surface area has been lost after NO_2 adsorption on HKUST-1 and MG-2, while on MG-1 a 50% decrease was found. The extent of the decrease in the volume of micropores (in terms of percentage) is similar to that of surface area. Surprisingly, a significant increase, even up to seven times in the volume of mesopores for the composite materials used in dry conditions, is revealed. On HKUST-1, regardless the conditions of the breakthrough test, the volume of mesopores increases only slightly. The trend is similar to that one found

Table 2. Parameters of the Porous Structure for the HKUST-1, MG-1, MG-2, and MG-3 Materials

sample	S_{BET} (m^2/g)	V_t (cm^3/g)	V_{mic} (cm^3/g)	V_{meso} (cm^3/g)	V_{mic}/V_t (%)	d^a (nm)	$S_{th}{}^b$ (m^2/g)	S_{th}/S_{BET}
HKUST-1	909	0.471	0.449	0.022	95	1000	6035	6.6
HKUST-1 ED	63	0.086	0.036	0.05	42			
HKUST-1 EM	753	0.411	0.361	0.05	89			
MG-1	989	0.515	0.478	0.037	93	950	6819	6.9
MG-1 ED	273	0.333	0.099	0.234	30			
MG-1 EM	418	0.271	0.194	0.077	72			
MG-2	1002	0.527	0.478	0.049	91	980	7562	7.5
MG-2 ED	159	0.251	0.062	0.189	25			
MG-2 EM	811	0.434	0.392	0.042	90			
MG-3	996	0.566	0.522	0.044	92	1310	6216	6.1
MG-3 ED	146	0.208	0.064	0.144	31			
MG-3 EM	738	0.356	0.307	0.049	86			

[a] Particles size calculated from X-ray line broadening and the Scherrer equation. [b] Specific surface area calculated assuming cubic particles of size *d*.

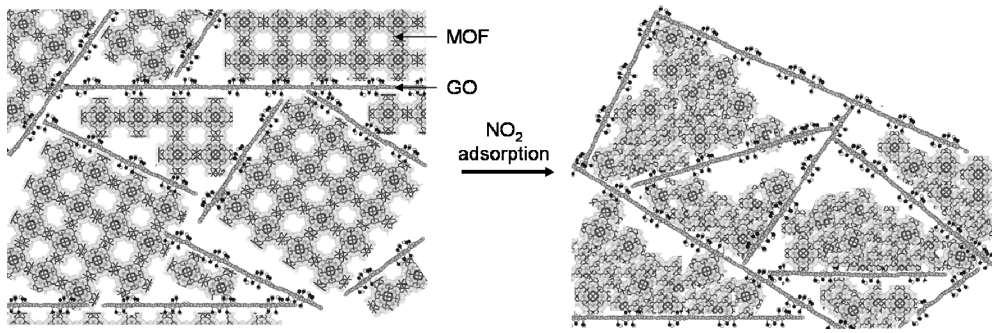

FIGURE 4. Changes in the texture of the composite materials after exposure to NO_2.

for each composite in moist conditions. Those changes in the porosity of the composites in dry conditions suggest that the layers of GO somehow determine the structure of the materials and the mesoporosity is likely formed between the units of collapsed HKUST-1 attached to the graphene layers. The changes in the texture are visualized in Figure 4.

The decrease in the surface area in dry and moist conditions is in agreement with the partial damage of the structure after NO_2 exposure, observed on XRD diffractograms. We hypothesize that binding between NO_2 and copper is responsible for the observed changes. Since this binding is limited in moist conditions, due to the competitive adsorption of water and NO_2 on copper, and thus, "screening" of some copper centers from NO_2, the surface areas are less affected. Moreover, the results suggest that the organic network is also affected by the NO_2 adsorption on copper, since only broken bonds in the lattice of the MOF (for instance, the linkage between copper centers and BTC) can explain the loss of the microporous volume. However, due to the differences in the texture, the destruction of the micropores is manifested differently for HKUST-1 than for the composites. For the latter materials, the "densification/agglomeration" of the HKUST-1 component leads to the creation of mesopores, since the units of MOF are enclosed between GO layers (Figure 4). Thus, the addition of GO confers to the composite materials an apparent stability, and the loss of micropores does not necessarily lead to a dramatic decrease of the surface area as that found for HKUST-1.

To further analyze the mechanism of reactive adsorption, the hypothetical surface of the materials, S_{th}, was calculated using eq 1 where *D* is the density of the material and cubic particles of size *d* are assumed (listed in Table 2), which is the size of the particles evaluated from X-ray diffraction data using the Scherrer equation (46).

$$S_{th} = \frac{6\sqrt{3}}{Dd} \quad (1)$$

This value (S_{th}) represents the theoritical surface of the materials in the case where all the crystallites are separated from each other. The dependence of the NO_2 adsorption capacity on the ratio of these values to the specific surface areas (S_{th}/S_{BET}) is analyzed (Figure 5). That S_{th}/S_{BET} ratio might be considered as an indication of the densification of the material particles (47). When this ratio is smaller and hypothetically reaches 1, the grains of materials are well separated from each other. Any increase of this value reflects a densification of the crystallites and the formation of particle boundary. The linear correlation ($R^2 = 0.93$) seen in Figure 5 for the experiments run in moist conditions indicates that the adsorption of NO_2 is basically ruled by the volume or the surface of grain boundary. Moreover, since NO_2 is known to be adsorbed in the micropores of carbonaceous materials (48−50), it is plausible to assume that between the particles/on the grain boundary the micropores enhancing the physisorption of NO_2 exist. As found, on the

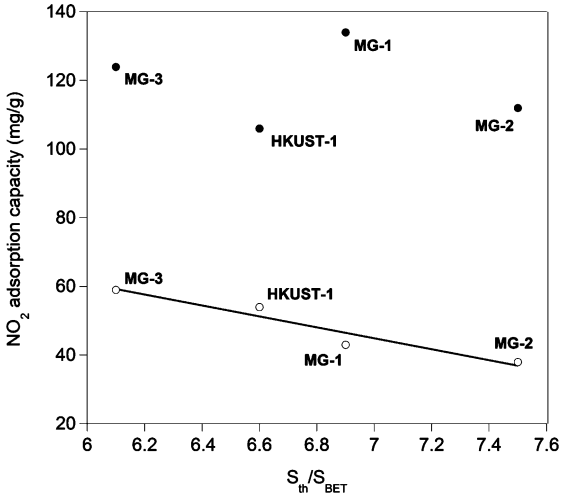

FIGURE 5. Correlation between NO_2 adsorption capacity in dry (●) and moist (○) conditions and S_{th}/S_{BET}.

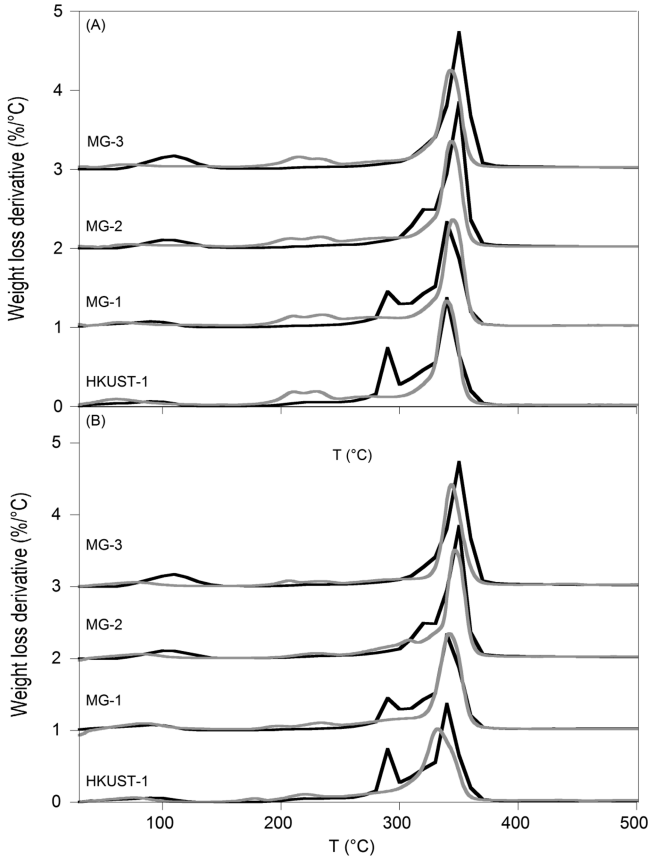

FIGURE 6. DTG curves of initial (black lines) and exhausted (gray lines) HKUST-1, MG-1, MG-2, and MG-3 samples in (A) dry and (B) moist conditions.

basis of the results of N_2 adsorption and XRD, this kind of adsorption is less destructive than the direct binding on copper (as observed in dry conditions). Water molecules act as a shield to prevent the destructive adsorption of NO_2 on Cu sites.

Thermal analyses were carried out on the initial and exhausted samples. The DTG curves are shown in Figure 6. Only the temperature range between 150 and 500 °C is included since at the temperatures lower than 150 °C only physically adsorbed species are removed and no visible

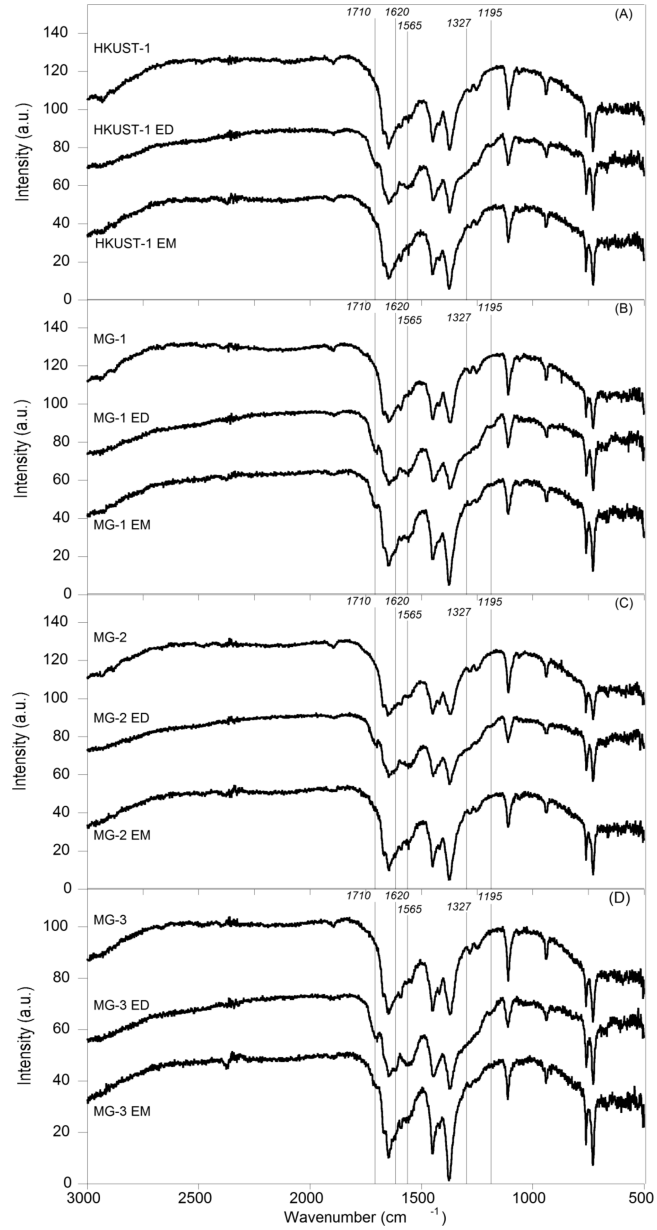

FIGURE 7. FTIR spectra of (A) HKUST-1, (B) MG-1, (C) MG-2, and (D) MG-3 before and after exposure to NO_2.

changes are seen at the temperatures higher than 500 °C. On the curves for the initial samples, a main peak, which is assigned to the decomposition of MOF, appears around 350 °C, and a smaller signal, slightly before 300 °C (only on HKUST-1 and MG-1), is linked to the release of water from the structure (34, 51). On the DTG curves for the exhausted samples, the main peak at around 350 °C remains, regardless of the experimental conditions. However, a small shift to a lower temperature and a decrease in the intensity of this signal are observed for MG-2 and MG-3 in dry and moist conditions and only in moist conditions for HKUST-1. This shift might be the result of a partial destruction of the material framework during the adsorption process. The peak centered around 300 °C seen on DTG curves of the initial HKUST-1 and MG-1 samples is no longer visible for the exhausted materials. New peaks appear around 200 and 230 °C on each DTG curve for the samples run in dry and moist

conditions. On the basis of the possible chemistry of the reactive adsorption process and the decomposition temperatures of the likely reaction products, these peaks are linked to the presence of nitrates ($Cu(NO_3)_2$) (52) and/or hydroxide ($Cu(OH)_2$) (53). For the samples exhausted in dry conditions, they should obviously represent the decomposition of the copper−nitrate complex, since without water copper hydroxide would not be formed. In moist conditions, since we consider that the competitive adsorption led to a preferable adsorption of water than of NO_2 on the copper centers, copper hydroxide should be the complex rather formed.

FTIR analysis brings additional details concerning complexes formed during the NO_2 reactive adsorption process. On the spectra for the materials exhausted in dry conditions (Figure 7), two new bands located at 1710 cm^{-1} and around 1327 cm^{-1} confirm the formation of nitrate bound to the copper (44). Moreover, the absence of this band on the spectra of the exhausted samples in moist conditions is other evidence that the presence of water prevents the interactions of NO_2 with the copper centers. The appearance of another new band at 1620 cm^{-1} only on the exhausted samples after the dry runs indicates the bidentate nature of the nitrates formed (44).

Considering all the results addressed above, the following mechanism is proposed to describe the reactive adsorption of NO_2 in dry conditions on the HKUST-1 and its composites with GO.

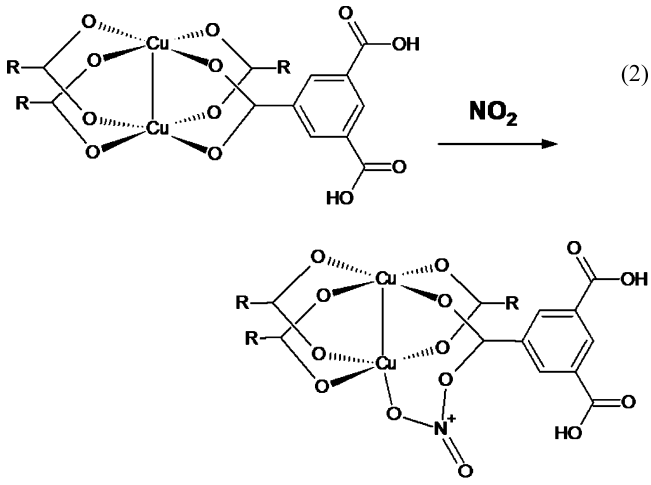

(2)

with R = benzene di-carboxylic.

As indicated above, the formation of a bidentate nitrate is supported by FTIR analysis (bands at 1710, 1620, and 1327 cm^{-1}). Such reaction requires the breaking of a Cu−O bond, which consequently induces a loss of microporous volume (Table 2) and a partial collapse of the main structure (observed on XRD diffractograms; eq 2). However, a second coordination may also occur since a small band at 1195 cm^{-1} indicates that nitrate species can be bound with two different metallic centers (54). A second step in this mechanism may be considered since an increase in the intensity of the band at 1565 cm^{-1} (Figure 7) is linked to a change in the coordination of the carboxylate ligands from benzene tricarboxylic (51). This step likely involves a second NO_2 molecule and leads to the formation of a monodentate nitrate bound to the copper (eq 3). This rearrangement may cause the appearance of carboxylic groups on benzene tricarboxylic linkage and the formation of NO, which is observed to be released in each case during the NO_2 adsorption process in dry conditions (eq 4).

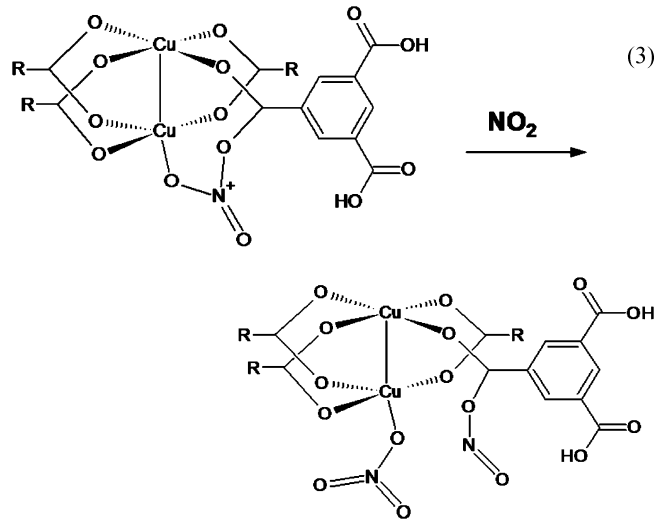

(3)

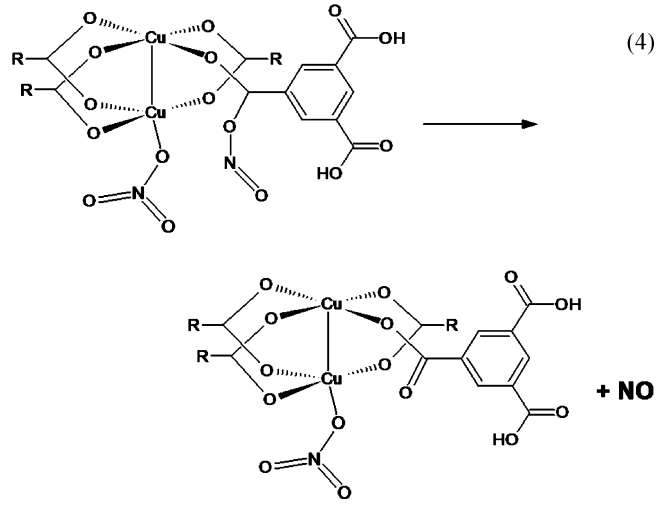

(4)

Concerning the FTIR spectra of the exhausted samples after the exposure to NO_2 in moist conditions, no significant change was observed in comparison with the initial samples. This clearly indicates that the mechanism represented above mainly takes place in dry conditions. In moist conditions, the presence of water hinders the adsorption of NO_2 on the copper as it was previously suggested. Thus, physical adsorption in small micropores is the main mechanism of the removal process.

4. CONCLUSIONS

The results presented in this paper show that the HKUST-1/GO composites exhibit significantly increased adsorption of NO_2 in dry conditions compared to the parent components. This is owing to an additional pore space formed between the HKUST-1 units and graphene units. The NO_2

adsorption mechanism on HKUST-1 and its composites with GO is very dependent on the presence of water. Taking into account the experimental results, two reaction pathways are proposed. In moist conditions, water is preferentially adsorbed on the copper centers and then reacts with them forming complexes. This reaction prevents the reactive adsorption of NO_2. When the number of copper sites for NO_2 interactions is reduced, less NO is released. However, a simple proportionality is not expected here since the adsorption of NO_2 is achieved in different manners including the adsorption on the copper sites but also in the micropores of the MOF or at the interface between MOF and GO. Lack of copper/NO_2 interactions also results in a more stable structure. Nevertheless, since less copper sites are available for interactions with NO_2, the adsorption capacity of HKUST-1 and its composites is lowered in comparison with that in dry conditions. Experiments in moist conditions also indicate that NO_2 adsorption is enhanced when the particles are close to each other, and thus, small micropores are formed where that NO_2 can be adsorbed physically. In dry conditions, the availability to the copper increases the density of active sites, and thus, more NO_2 is retained via reactive adsorption. The adsorption and disproportionation reactions of NO_2 accompanied by the release of NO result in a partial destruction of the porosity.

Acknowledgment. This study was supported by the ARO (Army Research Office) Grant W911NF-10-1-0030 and NSF collaborative Grant 0754945/0754979.

REFERENCES AND NOTES

(1) Liu, P. I. *Energy, technology, and the environment*; ASME Press: New York, NY; 2005.
(2) Manahan, S. H. In *Environmental Chemistry*, 8th ed.; Manahan, S. H., Ed.; CRC Press: Boca Raton, FL, 1997; p 310−317.
(3) Granger, P.; Pârvulescu, V. *Past and present in DeNOx catalysis: from molecular modelling to chemical engineering*; Elsevier: Amsterdam, 2007.
(4) Madia, G.; Koebel, M.; Elsener, M.; Wokaun, A. *Ind. Eng. Chem. Res.* **2002**, *41*, 4008–4015.
(5) Neathery, J. K.; Rubel, A. M.; Stencel, J. M. *Carbon* **1997**, *35*, 1321–1327.
(6) Kong, Y.; Cha, C. Y. *Carbon* **1996**, *34*, 1027–1033.
(7) Zhu, Z.; Liu, Z.; Liu, S.; Niu, H. *Fuel* **2000**, *79*, 651–658.
(8) Illán-Gómez, M. J.; Brandán, S.; Salinas-Martínez de Lecea, C.; Linares-Solano, A. *Fuel* **2001**, *80*, 2001–2005.
(9) Lee, Y.-W.; Choi, D.-K.; Park, J.-W. *Carbon* **2002**, *40*, 1409–1417.
(10) Pietrzak, R.; Bandosz, T. J. *Environ. Sci. Technol.* **2007**, *41*, 7516–7522.
(11) Mochida, I.; Korai, Y.; Shirahama, M.; Kawano, S.; Hada, T.; Seo, Y.; Yoshikawa, M.; Yasutake, A. *Carbon* **2000**, *38*, 227–239.
(12) Gao, X.; Liu, S.; Zhang, Y.; Luo, Z.; Ni, M.; Cen, K. *Fuel Process. Technol.* **2011**, *92*, 139–146.
(13) Bashkova, S.; Bandosz, T. J. *J. Colloid Interface Sci.* **2009**, *333*, 97–103.
(14) Zhang, W.-J.; Bagreev, A.; Rasouli, F. *Ind. Eng. Chem. Res.* **2008**, *47*, 4358–4362.
(15) Rivallan, M.; Ricchiardi, G.; Bordiga, S.; Zecchina, A. *J. Catal.* **2009**, *264*, 104–116.
(16) Ahrens, M.; Marie, O.; Bazin, P.; Daturi, M. *J. Catal.* **2010**, *271*, 1–11.
(17) Shirahama, N.; Moon, S. H.; Choi, K.-H.; Enjoji, T.; Kawano, S.; Korai, Y.; Tanoura, M.; Mochida, I. *Carbon* **2002**, *40*, 2605–2611.
(18) Zhang, W.-J.; Bagreev, A.; Rasouli, F. *Ind. Eng. Chem. Res.* **2008**, *47*, 4358–4362.
(19) Carabineiro, S. A.; Bras Fernandes, F.; Vital, J. S.; Ramos, A. M.; Fonseca, I. M. *Appl. Catal., B* **2003**, *44*, 227–235.
(20) Illán-Gómez, M. J.; Linares-Solano, A.; Radovic, L. R.; Salinas-Martínez de Lecea, C. *Energy Fuels* **1996**, *10*, 158–168.
(21) Márquez-Alvarez, C.; Rodríguez-Ramos, I.; Guerrero-Ruiz, A. *Carbon* **1996**, *34*, 1509–1514.
(22) Oark, B.-J.; Park, S.-J.; Ryu, S.-K. *J. Colloid Interface Sci.* **1999**, *217*, 142–145.
(23) Davini, P. *Carbon* **2001**, *39*, 2173–2179.
(24) Abe, T.; Amagasa, Y.; Yoshihara, S.; Shirakashi, T. *Carbon* **2007**, *45*, 1717–1717.
(25) Seredych, M.; Bashkova, S.; Pietrzak, R.; Bandosz, T. J. *Langmuir* **2010**, *26*, 9457–9464.
(26) Stuart, J. *Chem. Soc. Rev.* **2008**, *32*, 276–288.
(27) Czaja, A. U.; Trukhan, N.; Muller, U. *Chem. Soc. Rev.* **2009**, *38*, 1284–1293.
(28) Li, J.-R.; Kuppler, R. J.; Zhou, H.-C. *Chem. Soc. Rev.* **2009**, *38*, 1477–1504.
(29) Wang, Q. M.; Shen, D.; Bülow, M.; Lau, M. L.; Deng, S.; Fitch, F. R.; Lemcoff, N. O.; Semanscin, J. *Microporous Mesoporous Mater.* **2002**, *55*, 217–230.
(30) Roswsell, J. L. C.; Yaghi, O. M. *Microporous Mesoporous Mater.* **2004**, *73*, 3–14.
(31) Britt, D.; Tranchemontagne, D.; Yaghi, O. M. *Proc. Natl. Acad. Sci. U.S.A.* **2008**, *105*, 11623–11627.
(32) Muller, U.; Schubert, M. M.; Yaghi, O. M. In *Handbook of heterogeneous catalysis, Chemistry and applications of porous materials*, 2nd ed.; Ertl, G., Knözinger, H., Schüth, F., Weitkamp, J., Eds.; Wiley-VCH: Weinheim, Germany, 2008; p 247−262.
(33) Petit, C.; Bandosz, T. J. *Adv. Mater.* **2009**, *21*, 4753–4757.
(34) Petit, C.; Burress, J.; Bandosz, T. J. *Carbon* **2010**, DOI: 10.1016/j.carbon.2010.09.059.
(35) Petit, C.; Bandosz, T. J. *Adv. Funct. Mater.* **2010**, *20*, 111–118.
(36) Petit, C.; Beacom, B.; Bandosz, T. J. *Langmuir* **2010**, *23*, 15302–15309.
(37) Bashkova, S.; Bandosz, T. J. *Ind. Eng. Chem. Res.* **2009**, *48*, 10884–10891.
(38) Seredych, M.; Bandosz, T. J. *J. Phys. Chem. C* **2007**, *111*, 15596–15604.
(39) Millward, A. R.; Yaghi, O. M. *J. Am. Chem. Soc.* **2005**, *127*, 17998–17999.
(40) Hummers, W. S.; Offeman, R. E. *J. Am. Chem. Soc.* **1958**, *8*, 1339.
(41) Dubinin, M. M. In *Chemistry and Physics of Carbon*; Walker, P. L., Ed.; M. Dekker: New York, 1966; Vol. 2, p 51−120.
(42) Prestipino, C.; Regli, L.; Vitillo, J. G.; Bonino, F.; Damin, A.; Lamberti, C.; Zecchina, A.; Solari, P. L.; Kongshaug, K. O.; Bordiga, S. *Chem. Mater.* **2006**, *18*, 1337–1346.
(43) Peterson, G. W.; Wagner, G. W.; Balboa, A.; Mahle, J.; Sewell, T.; Karwacki, C. J. *J. Phys. Chem. C* **2009**, *113*, 13906–13917.
(44) Ali, I. O. *Mater. Sci. Eng. A* **2007**, *459*, 294–302.
(45) Kante, K.; Deliyanni, E.; Bandosz, T. J. *J. Hazard. Mater.* **2009**, *165*, 704–713.
(46) Scherrer, P. *Nachr. Ges. Wiss. Gottingen, Math.-Phys. Kl.* **1918**, *2*, 98–100.
(47) Royer, S.; Bérubé, F.; Kaliaguine, S. *App. Catal., A: Gen.* **2005**, *282*, 273–284.
(48) Kaneko, K.; Imai, J. *Carbon* **1989**, *27*, 954–955.
(49) Kaneko, K. *Langmuir* **1987**, *3*, 357–363.
(50) Zhang, W. J.; Rabiei, S.; Bagreev, A.; Zhuang, M. S.; Rasouli, F. *App. Catal., B: Environ.* **2008**, *83*, 63–71.
(51) Nakamoto, K. Complexes of alkoxides, alcohols, ethers, ketones, aldehydes, esters and carboxylic groups. In *Infrared and Raman spectra of inorganic and coordination compounds*; Wiley, John and Sons: Hoboken, NJ, 2009; pp 62−67.
(52) Hu, X.; Lei, L.; Chu, H. P.; Yue, P. L. *Carbon* **1999**, *37*, 631–637.
(53) Liu, N.; Wu, D.; Wu, H.; Luo, F.; Chen, J. *Solid State Sci.* **2008**, *10*, 1049–1055.
(54) Underwood, G. M.; Miller, T. M.; Grassian, V. H. *J. Phys. Chem. A* **1999**, *103*, 6184–6190.

AM100790V